Experimental Charge Density and Neutron Structural Study of *cis*-$HMn(CO)_4PPh_3$: Comprehensive Analysis of Chemical Bonding and Evidence for a C−H···H−Mn Hydrogen Bond

Yuriy A. Abramov,[†,‡] Lee Brammer,*[,†] Wim T. Klooster,[§] and R. Morris Bullock[§]

Department of Chemistry, University of Missouri−St. Louis, 8001 Natural Bridge Road, St. Louis, Missouri 63121-4499, and Chemistry Department, Brookhaven National Laboratory, P.O. Box 5000, Upton, New York 11973-5000

Received August 12, 1998

The structure and bonding in *cis*-$HMn(CO)_4PPh_3$ have been studied by low-temperature neutron and high-resolution X-ray diffraction, the latter study using a charge-coupled device (CCD) area detector. A charge density analysis, including the deformation density, a full topological analysis of ρ, and selected topological analysis of $-\nabla^2\rho$, has been conducted. *cis*-$HMn(CO)_4PPh_3$ adopts an approximately octahedral geometry, the largest deviation being the C(1)−Mn−C(3) angle of 160.0(1)°. The hydride ligand (Mn−H(1), 1.573(2) Å) is nucleophilic in nature (i.e., hydridic, with an effective atomic charge of −0.4e) and makes a short contact (2.101(3) Å) with an electrophilic (+0.3e) ortho phenyl hydrogen. The electrostatic component of the $H^{\delta+}\cdots H^{\delta-}$ interaction energy is calculated to be 5.7 kcal/mol from the experimental data. This electrostatic evidence coupled with the geometry (C−H···H 129.0(2)° and H···H−Mn 126.5(1)°) and the identification of an H···H bond path in the charge density distribution strongly supports the characterization of this interaction as an intramolecular C−H···H−Mn hydrogen bond. Both the deformation density and the topological study clearly illustrate the σ-donor nature of both the H−Mn and Ph_3P−Mn interactions and the σ-donor/π-acceptor nature of the manganese−carbonyl bonds. The topological study further confirms the decrease in C−O bond order upon coordination to the metal and demonstrates for the first time by this method that the metal−ligand bonds, although showing characteristics of a closed-shell interaction, do have a significant dative covalent component to the bond. The latter is reinforced by a study of the derived Mn d-orbital populations, in which populations of the d_{z^2} and $d_{x^2-y^2}$ orbitals are significantly higher than would be predicted by a simple crystal field theory model of metal−ligand bonding.

Introduction

The field of experimental charge density study[1] got its start in the late 1960s and 1970s through the use of deformation densities to show the accumulation of electron density in bonding and nonbonding (lone pair) regions of molecular crystals. The advent of multipole models,[2] more accurate data collection, and faster computers has propelled the field forward, allowing the direct calculation of a variety of properties[3] related to the charge density from the multipole parameters that model the static charge density distribution in the crystal. More recently the approach developed by Bader and co-workers[4] of analyzing the topology of the total charge density has migrated from the theoretical branch to the experimental branch of the charge density field, and permits a method of analysis that is less model-dependent. Furthermore, on the experimental front, recent advances in instrumentation through the coming widespread use of area detectors promises to revolutionize the charge density field by reducing data collection times from weeks to days or even hours.[5−7]

To date, the emphasis in the charge density field has primarily been on small organic molecules of biological interest and the number of studies of organotransition metal compounds remains in the tens.[8] Similarly, although there have been a few recent

* Corresponding author. E-mail: lee.brammer@umsl.edu.
† University of Missouri−St. Louis.
‡ Present address: Department of Chemistry, State University of New York at Buffalo, Buffalo, New York 14260-3000.
§ Brookhaven National Laboratory.

(1) (a) Coppens, P. *X-ray Charge Densities and Chemical Bonding*; Oxford Science Publishing: Oxford, 1997. (b) Tsirelson, V. G.; Ozerov, R. P. *Electron Density and Bonding in Crystals;* Institute of Physics Publishing: Bristol, 1996.
(2) (a) Hirshfeld, F. L. *Acta Crystallogr.* **1971**, *B27*, 769. (b) Stewart, R. F. *Acta Crystallogr.* **1976**, *A32*, 565. (c) Hansen, N.; Coppens, P. *Acta Crystallogr.* **1978**, *A34*, 909.
(3) For example, see ref 1 and: (a) Coppens, P.; Guru Row, T. N.; Leung, P.; Stevens, E. D.; Becker, P. J.; Yong, Y. W. *Acta Crystallogr.* **1979**, *A35*, 63. (b) Stewart, R. F. *J. Chem. Phys.* **1972**, *57*, 1664. (c) Moss, G.; Feil, D. *Acta Crystallogr.* **1981**, *A37*, 414. (d) Stevens, E. D.; Delucia, M. L.; Coppens, P. *Inorg. Chem.* **1980**, *19*, 813. (e) Spackman, M. A.; Weber, H.-P.; Craven, B. M. *J. Am. Chem. Soc.* **1988**, *110*, 775. (f) He, X. M.; Swaminathan, S.; Craven, B. M.; McMullan, R. K. *Acta Crystallogr.* **1988**, *B44*, 271.
(4) (a) Bader, R. F. W. *Atoms in Molecules: A Quantum Theory;* International Series of Monographs in Chemistry 22; Oxford University Press: Oxford, 1990. (b) Bader, R. F. W.; Essen, H. *J. Chem. Phys.* **1984**, *80*,1943.
(5) References 5 and 6 report charge density studies using CCD area detectors based upon synchrotron and sealed-tube X-ray sources, respectively. (a) Korizánsky, T.; Flaig, R.; Zobel, D.; Krane, H.-G.; Morgenroth, W.; Luger, P. *Science* **1998**, *279*, 356. (b) Graafsma, H.; Svensson, S. O.; Kvick, Å. *J. Appl. Crystallogr.* **1997**, *30*, 957.
(6) (a) Macchi, P.; Proserpio, D. M.; Sironi, A. *J. Am. Chem. Soc.* **1998**, *120*, 1447. (b) Martin, A.; Pinkerton, A. A. *Acta Crystallogr.* **1998**, *B54*, 471.
(7) The feasibility of charge density studies using imaging plate area detectors has also been discussed; see: Bolotovsky, R.; Darovsky, A.; Kezerashvili, V.; Coppens, P. *J. Synch. Rad.* **1995**, *2*, 181.
(8) For example, see: Angermund, K.; Claus, K. H.; Goddard, R.; Krüger, C. *Angew. Chem., Int. Ed. Engl.* **1985**, *24*, 237.

10.1021/ic9809660 CCC: $15.00
Published on Web 11/10/1998

studies of the topology of the charge density based upon experimental work, only very recently did the first reports of such analyses of transition metal compounds begin to appear,[6a] though a number of theoretical studies have been published.[9,10] Furthermore, to our knowledge the application of a topological analysis of the Laplacian to a chemical bonding study has not previously been investigated *experimentally*. It is with this background in mind that we set about the present study, the first reported charge density study of a transition metal hydride compound.[11]

Transition metal hydrides have generated tremendous scientific interest over a number of decades, both for their remarkable diversity of structures[12] and for their versatility in chemical reactions.[13] Transition metal-catalyzed transformations of organic compounds, a mainstay of organometallic chemistry, generally involve addition or removal of hydrogen in some form from the organic substrate, so the participation of metal hydrides in such processes is almost inevitable. Such processes include both stoichiometric and catalytic reactions.[14] In the present study, the transition metal hydride complex was selected in part for its structural simplicity, but also because the complex contains ligands of different donor/acceptor capability, as well as anticipated differences in the relative σ and π components of M−L bonding. However, examination of the neutron structure suggested the possible presence of an intramolecular C−H···H−Mn hydrogen bond, a type of weak interaction of considerable current interest,[15] which could be examined for the first time by modern charge density methods and bonding analysis. This is the first of a series of studies currently in progress in our laboratory, examining, by means of the charge density, the bonding in organometallic complexes containing transition metal−hydrogen interactions.

Table 1. X-ray and Neutron Experimental Data

	X-ray	neutron
space group, Z	$P\bar{1}$, 2	$P\bar{1}$, 2
a, b, c (Å)	9.120(4), 10.281(4), 10.642(4)	9.047(4), 10.207(4), 10.567(4)
α, β, γ (deg)	95.525(3), 96.196(3), 93.051(3)	95.47(3), 96.22(4), 93.06(4)
V (Å^3)	985.4(11)	963.6(12)
cryst dimens (mm)	0.40 × 0.27 × 0.25	4.0 × 3.8 × 3.2
cryst color	colorless	yellow
μ (mm^{-1})	0.78	0.14
trans coeffs	0.751−0.890	0.656−0.723
diffractometer	Siemens CCD-based SMART	4-circle (HFBR beam port H6M)
temperature (K)	118(5)	123.0(5)
wavelength (Å)	0.710 73	1.0462(1)
no. of measd reflns	79 186	9737
no. of indep reflns	19 901	7510
no. of obsd reflns ($I > 1.5\sigma(I)$)	15 875	5813
R_{int}	0.029 for data ($F > 4\sigma(F)$)	0.059 (wR_{int} 0.021)

Experimental Section

Synthesis. *cis*-$HMn(CO)_4PPh_3$ was prepared from the reaction of $HMn(CO)_5$ with PPh_3 using a minor modification of a previously reported procedure.[16] IR (cyclohexane): ν(CO) 2061 (m), 1984 (s), 1968 (vs), 1957 (s) cm^{-1}, in agreement with the originally reported spectrum.[17] The large (∼52 mg) yellow crystal of *cis*-$HMn(CO)_4PPh_3$ used for neutron diffraction was grown by slow cooling of a toluene/hexane solution to −11 °C. The small colorless crystal used for the X-ray diffraction experiment was grown by vapor diffusion of hexane into a toluene solution of *cis*-$HMn(CO)_4PPh_3$ at 22 °C.

Neutron Data Collection. Neutron diffraction data were obtained on the four-circle diffractometer at beam port H6M of the High Flux Beam Reactor at Brookhaven National Laboratory as described for previous studies.[18] The crystal temperature was maintained at 123 ± 0.1 K using a DISPLEX model CS-202 closed-cycle refrigerator (APD Cryogenics, Inc.) and monitored with a Pt resistance thermometer. Cell constants of the title compound were determined from $\sin^2\theta$ values of 32 reflections ($42° < 2\theta < 59°$). Reflections were scanned for the hemisphere of reciprocal space, $+h, \pm k, \pm l$, for $6° < 2\theta < 110°$, using $\omega-2\theta$ step scans. Additional data were collected for $-h, \pm k, \pm l$, for $85° < 2\theta < 110°$. Reflection scan widths in 2θ were as follows: 4.0° for $2\theta < 50°$, and $(2.239 + 3.795 \tan(\theta))°$ for $2\theta > 50°$. Intensities of two reflections monitored every 200 reflections indicated excellent experimental stability throughout. Integrated intensities I_0 and variances $\sigma^2(I_0)$ were derived from the scan profiles as described previously.[18] A Lorentz correction and an analytical absorption correction[19] were applied. Averaging over 1795 symmetry-related reflections gave a weighted internal agreement factor on F^2 of 0.021. See Table 1 for details.

X-ray Data Collection. X-ray diffraction data were collected at 118(5) K using a Siemens CCD-based SMART diffractometer (Mo Kα radiation). A total of 11 008 frames of data were collected in 16 runs with 15 s exposure times and 0.3° frame (scan) widths in ω. The intensity data were integrated with the SAINT software package.[20] Different integration box sizes were used in attempts to improve the integration statistics for the high-angle reflections ($\sin\theta/\lambda \geq 0.80$ Å^{-1}), which appeared to be worse due to both expected statistical consider-

(9) (a) MacDougall, P. J. The Laplacian of the Electronic Charge Distribution. Ph.D. Thesis, Department of Chemistry, McMaster University, Hamilton, Ontario, Canada, 1989. (b) MacDougall, P. J.; Hall, M. B.; Bader, R. F. W.; Cheeseman, J. *Can. J. Chem.* **1989**, *67*, 1842. (c) MacDougall, P. J.; Hall, M. B. *Trans. Am. Crystallogr. Assoc.* **1990**, *26*, 105. (d) Bo, C.; Poblet, J. M.; Benard, M. *Chem. Phys. Lett.* **1990**, *169*, 89. (e) Low, A. A.; Kunze, K. L.; MacDougall, P. J.; Hall, M. B. *Inorg. Chem.* **1991**, *30*, 1079 (f) Bytheway, I.; Hall, M. B. *Inorg. Chem*. **1995**, *34*, 3741. (g) Neuhaus, A.; Veldkamp, A.; Frenking, G. *Inorg. Chem*. **1994**, *33*, 5278. (h) Lin, Z.; Bytheway, I. *Inorg. Chem*. **1996**, *35*, 594. (i) Gillespie, R. J.; Bytheway, I.; Tang, T.-H.; Bader, R. F. W. *Inorg. Chem*. **1996**, *35*, 3954. (j) MacDougall, P. J. Private communication.

(10) (a) Lin, Z.; Hall, M. B. *Inorg. Chem.* **1991**, *30*, 646. (b) Lin, Z.; Hall, M. B. *Inorg. Chem*. **1991**, *30*, 2569. (c) Lin, Z.; Hall, M. B. *J. Am. Chem. Soc.* **1992**, *114*, 2928. (d) Lin, Z.; Hall, M. B. *J. Am. Chem. Soc*. **1992**, *114*, 6574. (e) Lin, Z.; Hall, M. B. *Inorg. Chem*. **1992**, *31*, 4262. (f) Lin, Z.; Hall, M. B. *Organometallics* **1993**, *12*, 19. (g) Lin, Z.; Hall, M. B. *Organometallics* **1993**, *12*, 4046. (h) Song, J.; Hall, M. B. *J. Am. Chem. Soc*. **1993**, *115*, 327. (i) Barton, D. H.; Hall, M. B.; Lin, Z.; Parekh, S. I.; Reibenspies, J. *J. Am. Chem. Soc.* **1993**, *115*, 5056. (j) Song, J.; Hall, M. B. *Organometallics* **1993**, *12*, 3118. (k) Hertwig, R. H.; Koch, W.; Schröder, D.; Schwarz, H.; Hrušák, J.; Schwerdtfeger, P. *J. Phys. Chem.* **1996**, *100*, 12253.

(11) (a) We are aware of three, as yet unpublished, studies, namely, $HMn(CO)_5$,[7b] $HMoCp(CO)_3$,[7c] and $H_3Ru_3(CCl)(CO)_9$.[7d] (b) Cameron, R. P.; Stevens, E. D.; Sweany, R. L. *Am. Crystallogr. Assoc. Mtg.* **1990**, Abstr. PD07. (c) Cameron, R. P.; Stevens, E. D.; Sweany, R. L.; Koetzle, T. F. *Am. Crystallogr. Assoc. Mtg.* **1988**, Abstr. PB7. (d) Cited in Coppens, P. *Coord. Chem. Rev.* **1985**, *65*, 285.

(12) (a) Teller, R. G.; Bau, R. *Struct. Bonding* **1981**, *44*, 1. (b) Bau, R.; Drabnis, M. H. *Inorg. Chim. Acta* **1997**, *259*, 27.

(13) Bullock, R. M. *Comments Inorg. Chem.* **1991**, *12*, 1.

(14) (a) Collman, J. P.; Hegedus, L. S.; Norton, J. R.; Finke, R. G. *Principles and Applications of Organotransition Metal Chemistry*; University Science Books: Mill Valley, CA, 1987. (b) Dedieu, A., Ed. *Transition Metal Hydrides*; VCH: New York, 1992.

(15) (a) Crabtree, R. H.; Siegbahn, P. E. M.; Eisenstein, O.; Rheingold, A. L.; Koetzle, T. F. *Acc. Chem. Res*. **1996**, *29*, 348. (b) Richardson, T. B.; Koetzle, T. F.; Crabtree, R. H. *Inorg. Chim. Acta*, **1996**, *250*, 69.

(16) Booth, B. L.; Haszeldine, R. N. *J. Chem. Soc. (A)* **1966**, 157.

(17) Hieber, W.; Faulhaber, G.; Theubert, F. *Z. Anorg. Allg. Chem*. **1962**, *314*, 125.

(18) McMullan, R. K.; Epstein, J.; Ruble, J. R.; Craven, B. M. *Acta Crystallogr*. **1979**, *B35*, 688.

(19) (a) de Meulenaer, J.; Tompa, H. *Acta Crystallogr.* **1965**, *19*, 1014. (b) Templeton, L. K.; Templeton, D. H. *Abstr. Am. Crystallogr. Assoc. Mtg.* Storrs, CT, 1973; p 143.

(20) *SAINT*, Version 4.036; Siemens Analytical X-ray, Inc.: Madison, WI, 1995.

Table 2. Summary of Least-Squares Refinements

	X-ray I	X-ray II	neutron
sin θ/λ range ($Å^{-1}$)	0.05−1.00	0.05−0.80	0.05−0.79
no. of reflns used, n	15 875 ($F > 3\sigma(F)$)	7701 ($F > 3\sigma(F)$)	7490
no. of params, m	477	477	398
mode of refinement	$F > 3\sigma(F)$	$F > 3\sigma(F)$	F^2
weighting scheme, w	$(\sigma^2(F) + 0.0001F^2)^{-1}$		$(\sigma^2(F^2) + 0.0004F^4)^{-1}$
extinction formalism	Becker−Coppens, crystal type I[24]		
y_{min}	0.93	0.94	0.80
$R(F)^a$ or $R(F^2)^b$	0.050[a]	0.024[a]	0.060[b]
$wR(F)^a$ or $wR(F^2)^b$	0.034[a]	0.023[a]	0.066[b]
$S(F)^a$ or $S(F^2)^b$	1.34[a]	1.25[a]	1.10[b]

[a] $R(F) = \sum(||F_o| - |F_c||)/\sum|F_o|$, $wR(F) = [\sum w(|F_o| - |F_c|)^2/\sum w|F_o|^2]^{1/2}$, $S(F) = [\sum w(|F_o| - |F_c|)^2/(n - m)]^{1/2}$. [b] $R(F^2) = \sum(F_o^2 - F_c^2)/\sum F_o^2$, $wR(F^2) = [\sum w(F_o^2 - F_c^2)^2/\sum wF_o^4]^{1/2}$, $S(F^2) = [\sum w(F_o^2 - F_c^2)^2/(n - m)]^{1/2}$.

ation (i.e., diminished scattering) and possibly a poorer integration scheme for this region of reciprocal space. Integration yielded a total of 79 186 measured reflections, of which 19 901 were unique and 15 875 had $F > 3\sigma(F)$. Fifty standard frames of data in the low-angle region measured after every fourth run showed that the intensity decay was negligible over the relatively short time of the experiment. The unit cell dimensions were determined from a least-squares refinement using reflection centroids for 512 measured reflections with $I/\sigma(I) > 10$ and $24° < \theta < 30°$. An empirical absorption correction was performed using the SADABS program.[21] The experimental X-ray data are summarized in Table 1.

Neutron Structure Refinement. The atomic positions from a previous X-ray structure determination[22] were used as a starting model, which was refined by full-matrix least-squares[23] based on 7490 independent F_o^2 values. The scale factor was varied, together with positional and anisotropic displacement parameters for all atoms. A type I, isotropic, Lorentzian mosaic, extinction correction was included.[24] The model converged with $\Delta/\sigma < 0.1$; the final difference Fourier had no residual positive or negative peaks with scattering density exceeding 2% of that at the largest carbon atom peak. Refinement details are summarized in Table 2, and selected interatomic distances and angles are given in Table 3. A full listing of final structural parameters is deposited as part of the Supporting Information. The molecular structure of $HMn(CO)_4PPh_3$ based upon the neutron parameters is presented in Figure 1.

X-ray Charge Density Refinements. The Hansen−Coppens flexible multipole formalism,[2c] as implemented in the program MOLLY, was used for observed structure factor fitting. Within this approach, the crystal electron density is described by superposition of aspherical pseudoatoms with charge density modeled by a multipole expansion about free atoms:

$$\rho_k(\mathbf{r}) = P_c\rho_c(r) + P_v(r)\kappa^3\rho_v(r) + \sum_{l=1}^{4}\kappa'^3 R_l(\kappa' r)\sum_{m=-l}^{l} P_{lm}y_{lm}(\mathbf{r}/r) \quad (1)$$

Here ρ_c and ρ_v are spherically averaged free-atom Hartree−Fock core and valence densities normalized to one electron; y_{lm} are real spherical harmonic angular functions; R_l are normalized Slater-type radial functions:

$$R_l(r) = \frac{\alpha^{n_l+3}}{(n_l+2)!}\, r^{n_l}\, e^{-\alpha r} \quad (2)$$

and κ and κ' are dimensionless expansion−contraction parameters, which can be refined in the fitting procedure along with the populations P_v and P_{lm}. The core populations P_c were fixed at the appropriate values. The initial values of exponential coefficients, α, were taken from optimized Slater-type exponents.[25] The n_l values for the first-row atoms were taken from the work of Hansen and Coppens,[2c] and for the Mn and P pseudoatoms they were set to 4 for all l. For the hydrogen pseudoatoms $n_1 = 2$ was used, which resulted in empirically better fitting of the observed structure factors. Spherically averaged ρ_c and ρ_v densities were constructed from the published ground-state wave functions.[26] The multipole expansion (eq 1) was truncated at the hexadecapole level ($l_{max} = 4$) for the Mn pseudoatom, at the octapole level ($l_{max} = 3$) for the first-row pseudoatoms, and at the dipole level ($l_{max} = 1$) for the hydrogens. To decrease the number of variable parameters, the deformation densities of the second and third phenyl rings were constrained to that of the first ring. The multipoles of all carbon pseudoatoms in the latter were constrained to have mirror

Table 3. Selected Interatomic Distances (Å) and Angles (deg) from Neutron Refinement

Mn−H(1)	1.573(2)
Mn−P	2.305(2)
Mn−C(1)	1.828(2)
Mn−C(2)	1.802(2)
Mn−C(3)	1.827(2)
Mn−C(4)	1.819(2)
C(1)−O(1)	1.134(1)
C(2)−O(2)	1.136(1)
C(3)−O(3)	1.132(1)
C(4)−O(4)	1.140(1)
P−C	1.813(1)−1.816(1)
C−C	1.380(1)−1.396(1)
C−H	1.074(2)−1.085(3)
H(1)−Mn−C(1)	81.1(1)
H(1)−Mn−C(2)	90.4(1)
H(1)−Mn−C(3)	79.2(1)
H(1)−Mn−C(4)	176.4(1)
H(1)−Mn−P	84.2(1)
C(1)−Mn−C(2)	88.4(1)
C(1)−Mn−C(3)	160.0(1)
C(1)−Mn−C(4)	101.2(1)
C(1)−Mn−P	87.6(1)
C(2)−Mn−C(3)	88.3(1)
C(2)−Mn−C(4)	92.5(1)
C(2)−Mn−P	173.7(1)
C(3)−Mn−C(4)	98.7(1)
C(3)−Mn−P	93.7(1)
C(4)−Mn−P	93.1(1)
Mn−C(1)−O(1)	174.6(1)
Mn−C(1)−O(2)	179.7(1)
Mn−C(1)−O(3)	174.9(1)
Mn−C(1)−O(4)	177.6(1)
Mn−P−C	113.7(1)−116.9(1)
P−C−C	118.6(1)−122.4(1)
C−P−C	103.2(1)−103.7(1)
C−C−C	119.1(1)−120.6(1)
C−C−H	118.9(1)−120.9(1)

(21) (a) Sheldrick, G. *SADABS*, Version 2, 1995 (unpublished).[21b] (b) Based upon the method of Blessing, R. H. *Acta Crystallogr.* **1995**, A*51*, 33.
(22) Kwiatkowski, W.; Brammer, L. Unpublished results.
(23) Lundgren, J.-O. *UPALS Crystallographic Computer Programs*; Report UUIC-B13-4-05; Institute of Chemistry, University of Uppsala: Uppsala, Sweden, 1982 (modified Brookhaven National Laboratory, 1983).
(24) Becker, P. J.; Coppens, P. *Acta Crystallogr.* **1974**, *A30*, 129.
(25) Clementi, E.; Raymondi, D. L. *J. Chem. Phys.* **1963**, *38*, 2686.
(26) Clementi, E.; Roetti, C. *Atomic Data Nucl. Data Tables* **1974**, *14*, 177.

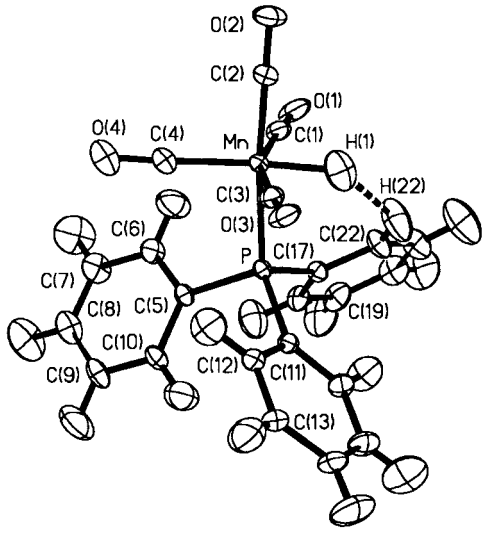

Figure 1. Molecular structure of $HMn(CO)_4PPh_3$ shown with 60% probability ellipsoids based upon the neutron refinement. Dashed line indicates C−H···H−Mn hydrogen bond.

symmetry in the corresponding phenyl ring plane, and the multipole parameters of the C(9), H(9), C(10), and H(10) pseudoatoms were constrained to equal those of the C(7), H(7), C(6), and H(6) pseudoatoms, respectively. Charge densities of all hydrogens, except hydride, H(1), were considered to have cylindrical symmetry along corresponding hydrogen−carbon bonds. The population of the diffuse 4s orbital of the Mn pseudoatom was considered to be zero, and the deformation density of the 3d orbitals was described using only monopole, quadrupole, and hexadecapole multipole parameters.[27] The neutrality constraint

$$\sum_j (Z_j - P_{cj} - P_{vj}) = \sum_j q_j = 0 \qquad (3)$$

was automatically applied during refinement. Here Z_j is the nuclear charge of the jth pseudoatom, q_j is the experimental jth pseudoatom charge, and summation is performed over all pseudoatoms in the unit cell. The site-symmetry-allowed multipole parameters were determined as described by Kurki-Sunio.[28] The total number of the variable electronic parameters was 223. Parameters were fitted using a least-squares minimizing function $\sum w(F_o - |F_m|)^2$, where F_o and F_m are observed and model structure factors, respectively, and $w = [\sigma^2(F_o) + 0.0001F_o^2]^{-1}$. The atomic anomalous dispersion parameters were taken from *International Tables for Crystallography*.[29]

Owing to the relatively poor integration statistics of the high-order reflections, two refinement series were carried out, first fitting the multipole model to all the observed structure factor data (refinement I), and second only to reflections with sin $\theta/\lambda \leq 0.80$ Å^{-1} (refinement II). It was noted previously[27] for dimanganese decacarbonyl that the Mn deformation charge density could be quite well studied even in the absence of high-order reflections (i.e., excluding data with sin $\theta/\lambda \geq 0.80$ Å^{-1}). The general scheme of refinement was as follows. First, the scale factor, extinction parameter, and non-hydrogen atom anisotropic displacement parameters were refined over all data. The coordinates of all atoms and anisotropic displacement parameters of the hydrogen atoms were fixed at the neutron diffraction experiment values at this stage. A high-order refinement (sin $\theta/\lambda \geq 0.60$ Å^{-1}) of the anisotropic displacement parameters of the non-hydrogen atoms was then performed. Subsequently, the multipole parameters and kappa parameters were introduced sequentially and refined for the non-hydrogen atoms over the data with sin $\theta/\lambda \leq 1.00$ Å^{-1}, and for the hydrogen atoms over low-angle (sin $\theta/\lambda \leq 0.50$ Å^{-1}) reflections. In the final step the coordinates of the non-hydrogen atoms were allowed to refine. Refinement II started from the parameters obtained during refinement I. The refinement was repeated over the observed structure factor data with sin $\theta/\lambda \leq 0.80$ Å^{-1}, within the same scheme. A summary of the least-squares refinements is presented in Table 2. The final electronic and structural parameters after refinement I and II appear to be close to each other. These data are deposited as part of the Supporting Information.

The neutron and X-ray diffraction experiments gave atomic positional parameters that are in very good agreement yielding almost indistinguishable crystal structures. However, the X-ray displacement parameters U_{ij} are significantly lower than the corresponding values derived from the neutron data. Such disagreement is quite common due to the differences in the various systematic errors (thermal diffuse scattering, temperature of the experiment, measurement errors, etc.) and can be avoided only at very low temperatures.[30] However, we can offer no satisfactory interpretation at present of the disagreement between the unit cell parameters derived from two experiments. The direction of this disagreement is opposite to that for the atomic displacement parameters. It should be noted that an independent X-ray study[22] of a similar crystal at 123(5) K using a Siemens P4 point detector diffractometer gave unit cell parameters that coincide with the present X-ray results within three esds.

The satisfactory quality of the multipole model fitting to the observed structure factors is reflected by the residual density:

$$\Delta\rho(\mathbf{r}) = V^{-1} \sum_{\mathbf{h}} [F(\mathbf{h}) - F_m(\mathbf{h})]\, e^{-2\pi i \mathbf{hr}} \qquad (4)$$

which is relatively low and featureless (see Supporting Information). Here F and F_m are, respectively, observed and model structure factors for the reciprocal lattice vector **h** and **V** is the volume of the unit cell.

Results and Discussion

In an effort to perform a comprehensive experimental study of the chemical bonding in the $HMn(CO)_4PPh_3$ molecule in its crystal environment, different methods of analysis have been applied independently to the model experimental charge density. These are a traditional deformation charge density analysis, a d-orbital occupancy study of the Mn atom from the refined multipole parameters,[27] and a quantum-topological analysis[4a] of the total crystal charge density and of its Laplacian.

Molecular and Crystal Structure. $HMn(CO)_4PPh_3$ adopts an approximately octahedral structure, the principal deviations being the orientation of carbonyls, C(1)[O(1)] and C(3)[O(3)], and the phosphine toward the hydride ligand and away from carbonyl C(4)[O(4)] [C(1)−Mn−C(3), 160.0(1)°, and H1−Mn−P, 84.2(1)°]. The reduction in the C−M−C angle of the carbonyls cis to the hydride is observed in $HMn(CO)_5$ and all other reported *trans*-$HML(CO)_2(PR_3)_2$ structures (M = Cr, Mn, Fe; L = CO, NO^+, I^-, $SiPh_3^-$),where corresponding angles range from 150.9 to 167.4°.[31] Reported angles for $HML(CO)_2(PR_3)_2$ (M = Re, W) are slightly larger at 159.7−170.0°, and those for related $XM(CO)_5$ and *cis*-$XML(CO)_4(PR_3)$ structures (X = Cl, Br, I; M = Cr, Mn, W, Re) are still larger at 172.3−

(27) Holladay, A.; Leung, P. C.; Coppens, P. *Acta Crystallogr.* **1983**, *A39*, 377.
(28) Kurki-Suonio, K. *Isr. J. Chem.* **1977**, *16*, 115.
(29) *International Tables for Crystallography*; Kluwer: Dordrecht, 1992; Vol. C.
(30) Iversen, B. B.; Larsen, F. K.; Figgis, B. N.; Reynolds, P. A.; Schultz, A. J. *Acta Crystallogr.* **1996**, *B52*, 923.
(31) (a) $HMn(CO)_5$ [164.0, 167.4°]: La Placa, S. J.; Hamilton, W. C.; Ibers, J. A.; Davison, A. *Inorg. Chem.* **1969**, *8*, 1928. (b) $HFe(CO)_2(SiPh_3)(P(OPh)_3)_2$ [150.9°]: Connolly, J. W.; Hatlee, M. J.; Cowley, A. H.; Sharp, P. R. *Polyhedron* **1991**, *10*, 841. (c) $HCr(NO)(CO)_2(PPh_3)_2$ [153.7°]: Peters, J. C.; Hillhouse, G. L.; Rheingold, A. L. *Polyhedron* **1994**, *13*, 1741. (d) $HMn(CO)_3(PPh_3)_2$ [158.5°]: Hayakawa, H.; Nakayama, H.; Kobayashi, A.; Sasaki, Y. *Bull. Chem. Soc. Jpn.* **1978**, *51*, 2041. (e) $HFeI(CO)_2(PPh_3)_2$ [159.0°]: Begley, M. J.; Puntambekar, S. G.; Wright, A. H. *J. Organomet. Chem.* **1987**, *329*, C7.

189.0°.[32] The approximate C_s molecular symmetry gives rise to three distinct carbonyl groups, the aforementioned pseudo-trans pair, the carbonyl trans to the phosphine, C(2)−O(2), and that trans to the hydride, C(4)−O(4). Slightly longer C−O distances and shorter Mn−C separations are observed for the carbonyls trans to the two ligands of greatest *trans*-influence, H and PPh_3, though the differences are small (<0.03 Å). The Mn−H distance of 1.573(2) Å is comparable to the 1.601(16) Å separation observed in the only other neutron diffraction study of a terminal Mn−H bond, for β-$HMn(CO)_5$.[31a]

There are no unusual intermolecular contacts. However, a short intramolecular contact between the ortho hydrogen (H(22)) of one of the phenyl rings and the hydride [H(22)···H(1) 2.101(3) Å] warrants further consideration. Richardson, Koetzle, and Crabtree have examined geometrically similar intramolecular interactions in a survey[15b] of neutron diffraction and low-temperature X-ray diffraction studies of cis transition metal phosphine hydrides and related compounds. They suggest that these contacts may correspond to weak C−H···H−M hydrogen bonds analogous to X−H···H−M (X = O, N) interactions recently characterized.[15a] In the present structure, the C(22)−H(22)···H(1) angle of 129.0(2)° and the Mn−H(1)···H(22) angle of 126.5(1)° lie within one standard deviation of the mean values given by Crabtree and co-workers [C−H···H, 142(14)°; M−H···H, 130(14)°] for a set of over 40 proposed C−H···H−M hydrogen bonds. In addition, the torsion angle Mn−H(1)···H(22)−C(22) is only 0.7(3)°, indicating coplanarity of the Mn−H(1) and C(22)−H(22) bonds. The geometry of the related *cis*-$ClMn(CO)_4PPh_3$ [H···Cl, 2.510 Å; C−H···Cl, 146.7°; M−Cl···H, 89.4°; Mn−Cl···H−C 20.6°][33] is quite consistent with an intramolecular C−H···Cl−Mn hydrogen bond, lending further support to characterization of the C(22)−H(22)···H(1)−Mn interaction in *cis*-$HMn(CO)_4PPh_3$ as a hydrogen bond. Still stronger evidence supporting this assignment comes from the experimental atomic charges and the topological analysis of the charge density distribution (vide infra).

Atomic Charges and Electrostatic Interaction Energy. Information on charge transfer between atoms can be found from the pseudoatom effective charges, q_j, which give a relative estimation of this effect between interacting atoms in the crystal. This is elaborated upon by a consideration of the deformation density (vide infra). The experimental effective charges in the $HMn(CO)_4PPh_3$ molecule in the crystal are presented in Table 4. Of particular interest is the charge on the hydride. The magnitude of the charge associated with metal hydrides, and even its sign in the case of more acidic hydrides, has been the subject of intense speculation and investigation over the years,[34] particularly as this pertains to the transfer of hydrogen (hydride, proton or hydrogen atom) through cleavage of the M−H bond.[13] We are not aware of any previous determinations of the hydride charge for $HMn(CO)_4PPh_3$, though both theoretical[34a] and experimental[34b,c] means have indicated that the hydride carries a negative charge in the related $HMn(CO)_5$. For the latter, estimates include −0.3e from SCF calculations,[34a] a range of −0.1 to −0.4e from NMR measurements,[34b] which when compared with the present determination conform to the idea that *cis*-$HMn(CO)_4PPh_3$ is more hydridic than $HMn(CO)_5$. Only the value derived from XPS core binding energies[34c] (−0.80 ± 0.24e for $HMn(CO)_5$) is not consistent with these observations. However, while it is tempting to associate hydride charge with hydride donor ability, it should be recognized that hydride transfer rates[35] should depend at best only in part upon the ground-state charge distribution.

Table 4. Experimental Effective Pseudoatom Charges for Selected Atoms (Electrons)[a]

pseudoatom	effective charge (e)
Mn	+1.65(2)
	+1.69(1)
H(1)	−0.40(5)
	−0.38(5)
P	+0.54(4)
	+0.59(4)
O(1)	−0.16(2)
	−0.15(2)
O(2)	−0.20(2)
	−0.19(2)
O(3)	−0.16(2)
	−0.15(2)
O(4)	−0.24(2)
	−0.23(2)
C(1)	−0.25(3)
	−0.28(2)
C(2)	−0.47(3)
	−0.46(3)
C(3)	−0.24(3)
	−0.27(2)
C(4)	−0.38(3)
	−0.37(2)
C(5) [C_{ipso}]	−0.20(2)
	−0.21(1)
C(6) [C_{ortho}]	−0.28(2)
	−0.28(1)
C(7) [C_{meta}]	−0.27(1)
	−0.26(1)
C(8) [C_{para}]	−0.23(2)
	−0.24(2)
H(6) [H_{ortho}]	+0.32(1)
	+0.31(1)
H(7) [H_{meta}]	+0.33(1)
	+0.32(1)
H(8) [H_{para}]	+0.32(1)
	+0.30(1)

[a] The first and second lines refer to the X-ray refinement I and II, respectively.

Finally, the relative experimental atomic charges clearly show that in the ground state the hydride is nucleophilic (charge −0.40(5)e) whereas the ortho phenyl hydrogen H(22) is electrophilic (charge +0.32(1)e), consistent with a weakly attractive electrostatic C(22)−H(22)···H(1)−Mn hydrogen bonding interaction. To further explore the nature of this interaction, the electrostatic component of the H(22)···H(1) interaction, E_{es}, has been evaluated through an expansion in terms of electrostatic multipole moments.[36] These moments can be obtained directly from the refined atomic charge density multipole moments.[1a] For the better convergence, all quadrupole moments on the H(1) and H(22) hydrogens were refined and these terms were included in an expansion of E_{es} up to the R^{-5} term. The electrostatic contribution to the hydrogen bond energy is thus calculated to be 5.7 kcal/mol. Although E_{es} is the leading bond energy term

(32) (a) From a survey of the Cambridge Structural Database (CSD).[32b] Angles exceeding 180° refer to carbonyl groups oriented away from the halogen. (b) Allen, F. H.; Kennard, O. *Chem. Des. Automation News* **1993**, *8*, 1 and 31−37.

(33) (a) Vahrenkamp, K. *Chem. Ber.* **1971**, *104*, 449. (b) Phenyl hydrogen atoms were placed in calculated positions with C−H 1.08 Å based upon reported non-hydrogen atom coordinates.[33a]

(34) (a) Guest, M. F.; Hall, M. B.; Hillier, I. H. *Mol. Phys.* **1973**, *25*, 629. (b) Lohr, L. L.; Lipscomb, W. N. *Inorg. Chem.* **1964**, *3*, 22. (c) Chen, H.-W.; Jolly, W. L.; Kopf, J.; Lee, T. H. *J. Am. Chem. Soc.* **1979**, *101*, 2607.

(35) (a) The rate of hydide transfer to the substrate Ph_3C^+ is ca. 5 times greater for *cis*-$HMn(CO)_4PPh_3$ than for $HMn(CO)_5$.[35b] (b) Cheng, T.-Y.; Bullock, R. M. *Organometallics* **1995**, *14*, 4031.

(36) Buckingham A. D. In *Intermolecular Interactions: From Diatomics to Biopolymers*; Pullman, B., Ed.; Wiley: New York, 1978; pp 1−67.

for medium-strength and weak hydrogen bonds, the total energy is expected to be smaller due to penetration and short-range repulsion effects.[37] Thus, in accordance with these considerations, the energy of the C−H···H−Mn hydrogen bond can be expected to be slightly less than that determined for the related N−H···H−El (El = M, B) hydrogen bonds[15a] (4−8 kcal/mol from spectroscopic measurements and DFT calculations).

Deformation Charge Density and d-Orbital Occupancies. The static deformation density is defined as the difference between the static multipole crystal model and that constructed from the corresponding free spherical atoms. Thus the deformation density shows the redistribution of the charge density in a crystal due to the interaction between atoms and can be very useful for chemical bonding studies of compounds in crystalline form. Regions of their positive deformation density indicate the accumulation of electronic charge in the crystal; depletion of charge is shown by negative deformation density. The sections of the $HMn(CO)_4PPh_3$ deformation density in the three different planes are shown in Figure 2.

The deformation density of the phenyl ring (Figure 2a) nicely illustrates the covalent bonding between neighboring carbon atoms. The deformation density maxima of ∼0.6−0.7 e Å^{-3} between carbons are in good agreement with the corresponding theoretical values for an aromatic ring.[38] Despite the charge transfer from the hydrogen atoms to carbons found in the phenyl rings (Table 4), the deformation density reveals an accumulation of charge at the hydrogen nuclei (Figure 2a). This relative effect can be accounted for by the significant contraction of the hydrogen pseudoatom valence density ($\kappa = 1.27(1)$, $\kappa' = 0.91(3)$) in the crystal (relative to the gas-phase free atom reference density) and is eliminated when the already contracted free hydrogen atom density[39] is chosen as the reference.

The Mn atom is of particular interest for a bonding study due to its coordination by three different types of ligand: the hydride, a strong σ-donor with no π-symmetry orbitals; the phosphine, a strong σ-donor and weak π-acceptor; and the carbonyls, generally regarded as moderate σ-donors and strong π-acceptors. The deformation density in the vicinity of the Mn atom, and the metal−ligand bonding region, is presented in Figures 2b and c. Substantial density accumulation both in the bonding and nonbonding (lone pair) regions of carbon and oxygen atoms in the carbonyl groups is revealed. The presence of the C≡O π-bonding interactions in the carbonyls is illustrated by the markedly elongated density accumulation between the atoms in the directions normal to the internuclear vector in contrast, for example, with the C−C σ-bond observed *in the plane* of the phenyl ring (Figure 2a). The lone pair density of the phosphorus atom directed toward the Mn atom is also reflected in the corresponding positive deformation density peak in Figure 2c, and the density of the hydride ligand appears to be noticeably polarized toward the Mn atom.

The Mn atom displays the following charge density redistribution in the crystal: the lobes of the electronic charge deficit (negative deformation density) are directed toward each ligand along the d-orbitals of (octahedral) e_g symmetry, while the excess charge (positive deformation density) is accumulated over d-orbital regions of (octahedral) t_{2g} symmetry, i.e., in the direction of the faces of the octahedron defined by the six ligands. The Mn d-orbital occupancies and spatial charge distribution can obviously be accounted for qualitatively by the

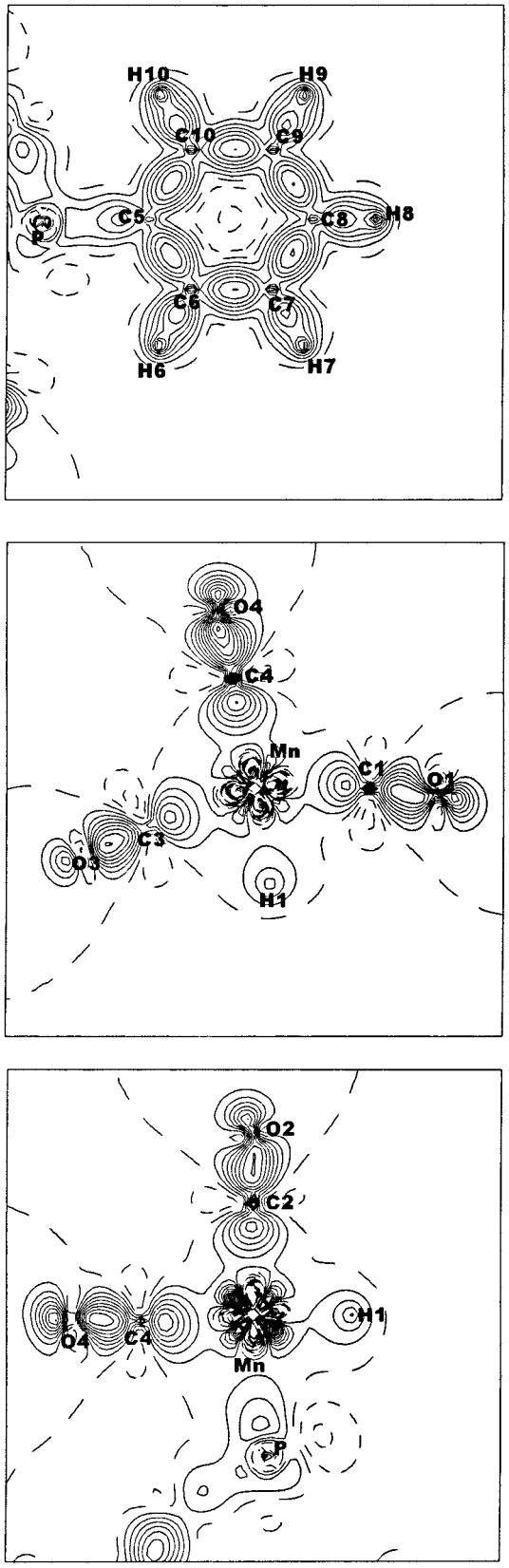

Figure 2. Static deformation charge densities in the planes defined by atoms: (a) C(5), C(8), C(10); (b) Mn, C(1), C(4); (c) Mn, H(1), C(2). Positive, negative, and zero contours are represented by solid, short-dashed, and long-dashed lines, respectively. Contour intervals are 0.1 e/Å^3. (Note that the uncontracted gas-phase hydrogen free atom has been used in calculation of the reference density; see text.)

(37) For example, see: Spackman, M. A.; Weber, H.-P.; Craven, B. M. *J. Am. Chem. Soc.* **1988**, *110*, 775.
(38) For example, see: Howard, S. T.; Hursthouse, M. B.; Lehmann, C. W.; Mallinson, P. R.; Frampton, C. S. *J. Chem. Phys.* **1992,** *97*, 5616.
(39) Stewart, R. F.; Davidson, E. R.; Simpson, W. T. *J. Chem. Phys.* **1965**, *42*, 3175.

Table 5. Occupancies of the Mn d-Orbitals[a] from Multipole Coefficients[27]

d-orbital populations (e, %)	refinement I	refinement II	O_h crystal field (for low-spin d^5)
$P(z^2)$	0.76(5), 14.2%	0.72(6), 13.6%	0%
$P(xz)$	1.37(6), 25.6%	1.36(6), 25.6%	33.3%
$P(yz)$	1.20(6), 22.4%	1.20(6), 22.6%	33.3%
$P(x^2 - y^2)$	0.81(5), 15.1%	0.79(6), 14.9%	0%
$P(xy)$	1.21(5), 22.6%	1.24(6), 23.4%	33.3%
total	5.35(2)	5.31(1)	5e
mixing terms			
$P(z^2/xz)$	−0.16(5)	−0.17(5)	
$P(z^2/yz)$	0.03(4)	0.07(5)	
$P(z^2/x^2 - y^2)$	−0.06(5)	−0.07(5)	
$P(z^2/xy)$	0.02(5)	0.00(5)	
$P(xz/yz)$	0.08(6)	0.08(6)	
$P(xz/x^2 - y^2)$	−0.08(6)	−0.07(6)	
$P(xz/xy)$	0.03(6)	0.07(6)	
$P(yz/x^2 - y^2)$	−0.08(6)	−0.07(6)	
$P(yz/xy)$	0.05(6)	0.00(6)	
$P(x^2 - y^2/xy)$	0.05(5)	0.04(6)	

[a] $\rho_d = \sum_{i=1}^{5} P_i d_i^2 + \sum_{i=1}^{5}\sum_{j>i}^{5} P_{ij}\, d_i\, d_j$; z axis is directed toward P; x axis is directed toward C(4).

crystal field effect in this distorted octahedral complex. A more detailed quantitative study of the d-orbital populations is presented below.

The fairly simple interpretation of the calculated deformation density distribution presented above clearly corresponds to the predominant simple donor−acceptor σ-interaction of Mn atom with all six ligands. That is, the lone pairs of the carbons and the phosphorus atoms as well as the hydride ion density donate their charges to the "vacant" e_g d-orbitals of the Mn atom. Within such an interatomic interaction scheme it is possible to neglect the two-center (i.e., shared covalent) contribution to the bond formation and evaluate the Mn atom d-orbital occupancies.[27] These orbital occupancies can be calculated due to the interrelation in this case between the transition metal atom multipole populations P_{lm} ($l = 0, 2, 4$), describing valence d-orbital charge density ρ_d as in eq 5, and its d-orbital occupancies P_i, describing ρ_d in the terms of atomic orbitals, d_i:

$$\rho_d = \sum_{i=1}^{5} P_i d_i^2 + \sum_{i=1}^{5}\sum_{j>i}^{5} P_{ij} d_i d_j \qquad (5)$$

The calculated occupancies using results of both refinement I and II are presented in Table 5. There is a good quantitative agreement between occupancies obtained from the two refinement schemes. The results obtained give a quantitative support to the qualitative considerations of the Mn−ligand interactions presented above. At present there are no theoretical data with which to directly compare these values for the $HMn(CO)_4PPh_3$ molecule.

There is also a less pronounced bonding effect which can be found in the deformation density maps (Figure 2b and c) and should be carefully analyzed. This is a weak charge accumulation connecting the Mn d-orbitals of t_{2g} symmetry with the edges of the carbon lone pairs in the carbonyls. The height of these deformation density maxima is slightly above 0.1 e $Å^{-3}$, which is quite close to the typical error in the deformation density in the valence region. However, this feature in the deformation charge density of a transition metal carbonyl complex has been previously interpreted as corresponding to π-back-donation from the metal.[1b] Within the well-established description of metal−carbonyl bonding, the carbonyl groups donate their carbon lone pair charge density to the Mn atom "vacant" d-orbitals of the e_g symmetry (σ-donation), while the Mn donates back the charge density from its "filled" t_{2g} d-orbitals to the vacant π^* antibonding molecular orbitals (MO) of the carbonyls (π-back-donation). The latter orbitals are predominantly located near the carbon atoms, which explains the observed effect in the deformation charge density (Figure 2b and c). Transition metal to carbonyl π-back-donation has been extensively studied both experimentally[40] and theoretically[41] in $Cr(CO)_6$ as a model system, and shows similar deformation density features. The same bonding picture was found also in $Mn_2(CO)_{10}$.[42] There are also several indirect signs of the metal−carbonyl π-back-donation in addition to the bridges of positive deformation density in the $HMn(CO)_4PPh_3$ molecule. One of them is the inversion of effective atomic charges in the carbonyls, wherein the carbons are more negatively charged than oxygen pseudoatoms (Table 4), due to the predominant concentration of the π^* MOs on the carbons. This effect was observed previously[42a] for the axial carbonyls in $Mn_2(CO)_{10}$. Perhaps most interesting is the observation that the occupancies of the Mn d_{yz}- and d_{xy}-orbitals (Table 5), involved in π-donation to three carbonyl ligands, are significantly less than that of the d_{xz}-orbital, which interacts with only two carbonyls.

Topological Analysis: General. Bader's topological analysis of the total charge density, ρ,[1,4a] suggests a model of the chemical bond that takes advantage of the interrelation between the charge density distribution, the local electronic energy and the chemical bond. This method does not rely on a reference density for analyzing the chemical bond. Thus it is free of some of the uncertainties of the deformation electron density approach.[43] Initially the topological approach was applied only to analyses of theoretical charge densities. Its application to experimental (X-ray diffraction) charge densities is now beginning to develop[44] due to the possibility of analytically representing the experimental charge density by various multipole techniques,[2] allowing analytical evaluation of the Laplacian, $\nabla^2\rho$, and gradient vector field of ρ, $\nabla\rho$. It was demonstrated recently[45] that this allows at least a semiquantitative study of the topological characteristics of highly accurate X-ray charge densities.

There are special points, called critical points (CP), in the charge density distribution at which the gradient of ρ, $\nabla\rho$, vanishes. These are of particular interest in the extraction of chemical information from the total charge density. Four possible types of nondegenerate CPs of ρ, which are labeled by their rank of 3 (i.e., 3 nonzero principal curvatures[46] of the charge density) and signature (algebraic sum of signs of these curvatures), correspond to maxima (3, −3), minima (3, +3), and saddle points (3, +1) and (3, −1) in the charge density. The definition and classification of the chemical bond in the

(40) Rees, B.; Mitschler, A. *J. Am. Chem. Soc.* **1976**, *98*, 7918.
(41) Sherwood, D.; Hall, M. B. *Inorg. Chem.* **1982**, *22*, 93.
(42) (a) Martin, M.; Rees, B.; Mitschler, A. *Acta Crystallogr.* **1982**, *B38*, 6. (b) Rosa, A.; Ricciardi, G.; Baerends, E. J.; Stukens, D. J. *Inorg. Chem.* **1995**, *34*, 3425.
(43) (a) For example, the diminished or nonexistent bonding electron peaks associated with bonds involving electron-rich atoms.[43b−d] (b) Savariault, J. M.; Lehmann, M. S. *J. Am. Chem. Soc.* **1980**, *102*, 1298. (c) Dunitz, J. D.; Seiler, P. *J. Am. Chem. Soc.* **1983**, *105*, 7056. (d) Dunitz, J. D.; Schweizer, W. B.; Seiler, P. *Helv. Chim. Acta* **1983**, *66*, 123 & 134.
(44) Tsirelson, V. G. *Can. J. Chem.* **1996**, *74*, 1171.
(45) Abramov, Yu. A.; Okamura, F. P. *Acta Crystallogr.* **1997**, *A53*, 187.
(46) Principal curvatures refer to the eigenvalues of the diagonalized matrix of second derivatives of ρ at the CP.

Table 6. Bond Critical Points of the Charge Density for Selected Bonds

bond (A−B)	R_{AB}[a] (Å)	R_A[b] (Å)	ρ (e/Å^3)	$\nabla^2\rho$ (e/Å^5)	λ_1 (e/Å^5)	λ_2 (e/Å^5)	λ_3 (e/Å^5)	ϵ
Mn−H(1)	1.58	1.03	0.651(21)	5.30(9)	−3.6	−3.5	12.4	0.03
Mn−P	2.33	1.08	0.520(4)	3.50(5)	−1.9	−1.8	7.2	0.04
Mn−C(1)	1.84	0.96	0.904(7)	10.81(14)	−4.7	−4.3	19.8	0.11
Mn−C(2)	1.82	0.94	0.999(7)	11.22(15)	−5.3	−4.9	21.4	0.06
Mn−C(3)	1.84	0.95	0.935(8)	10.66(21)	−4.8	−4.5	20.0	0.08
Mn−C(4)	1.84	0.94	0.986(7)	11.42(16)	−5.1	−5.0	21.5	0.02
O(1)−C(1)	1.14	0.76	3.191(20)	8.40(77)	−31.3	−30.4	70.0	0.03
O(2)−C(2)	1.15	0.76	3.203(26)	7.11(99)	−30.3	−28.9	66.3	0.05
O(3)−C(3)	1.14	0.76	3.205(21)	16.58(85)	−33.0	−31.1	80.7	0.06
O(4)−C(4)	1.15	0.76	3.237(27)	10.11(127)	−32.6	−31.8	74.5	0.03
P−C(5)	1.83	0.84	1.104(25)	−4.35(84)	−5.3	−4.7	5.7	0.12
P−C(11)	1.83	0.84	1.129(18)	−4.93(53)	−5.4	−5.1	5.6	0.07
P−C(17)	1.83	0.84	1.044(34)	−3.65(98)	−5.0	−4.6	6.0	0.10
C(5)−C(6)	1.40	0.69	2.150(9)	−19.24(4)	−15.7	−13.1	9.6	0.20
C(6)−C(7)	1.40	0.68	2.190(9)	−20.50(15)	−16.0	−13.6	9.2	0.18
C(7)−C(8)	1.40	0.70	2.199(14)	−20.42(18)	−16.3	−13.6	9.4	0.20
C(8)−C(9)	1.39	0.70	2.201(12)	−20.60(3)	−16.2	−13.7	9.3	0.18
C(9)−C(10)	1.40	0.71	2.177(10)	−20.17(17)	−15.9	−13.5	9.3	0.18
C(10)−C(5)	1.40	0.71	2.154(12)	−19.54(15)	−15.7	−13.2	9.4	0.19
H(6)−C(6)	1.09	0.32	1.751(22)	−13.05(21)	−17.2	−16.4	20.6	0.05
H(7)−C(7)	1.10	0.32	1.690(21)	−12.17(19)	−16.4	−15.8	20.0	0.04
H(8)−C(8)	1.09	0.32	1.721(27)	−12.73(21)	−16.8	−16.1	20.1	0.04
H(9)−C(9)	1.08	0.32	1.725(30)	−12.90(33)	−16.9	−16.3	20.2	0.04
H(10)−C(10)	1.08	0.32	1.795(29)	−14.02(30)	−17.8	−17.0	20.8	0.05
H(22)···H(1)	2.12	1.07	0.066(5)	0.79(3)	−0.25	−0.18	1.22	0.40

[a] Interatomic distance. Distances are calculated from coordinates used in charge density refinement and differ from those calculated using neutron coordinates (Table 3) by less than 1%. [b] Distance between critical point and nucleus of atom A.

topological analysis of ρ are based on the existence of a (3, −1) CP between neighboring atoms and on the properties of charge density at this point.[4a] This point is characterized by the one positive principle curvature, λ_3, along the internuclear line and negative principle curvatures, λ_1 and λ_2, in the two perpendicular directions.

Bader has proposed[4a] that the occurrence of (3, −1) CPs between any atoms in a system under equilibrium is necessary and sufficient for chemical bonding between these atoms and that the critical point in this case be referred to as a *bond* critical point (BCP). However, we will take the less rigid interpretation that, while such a critical point is typically associated with what chemists view as a chemical bond between atoms and may even be a necessary condition for bonding, it is clearly not a sufficient condition as has been demonstrated in instances where such critical points characterize *repulsive* interatomic interactions between second-neighbor atoms (ions).[47] Within the scheme of topological analysis described, a relatively high charge density and negative sign of the Laplacian of ρ (second derivative, $\nabla^2\rho$) at the BCP are considered to characterize a shared (covalent) bond, while a low ρ and a positive value of $\nabla^2\rho$ indicates a closed-shell interaction (i.e., ionic, hydrogen bond or van der Waals interaction). These represent the extreme descriptions within the scheme and it should be anticipated that as in any other description scheme for chemical bonds there should be a range of examples that lie between the extremes.

Our efforts to undertake a comprehensive topological study of the reported experimental charge density and of its Laplacian is presented below. It should be noted that to date a number of theoretical studies of the topology of ρ,[9,10] but few of the topology of $\nabla^2\rho$,[9a−c] of transition metal-containing systems have been published. A locally modified version of program LSPROP[48] was used to search for and analyze critical points and for calculation of the $\nabla^2\rho$ distribution. Within this program, variance−covariance matrix elements of all multipole parameters are used for the calculation of the variance in the charge density property. The properties of the experimental ρ at the BCPs for selected bonds in the $HMn(CO)_4PPh_3$ molecule are presented in Table 6. The maps of the $-\nabla^2\rho$ distribution in the $HMn(CO)_2P$ plane and phenyl ring plane are presented in Figure 3.

Topological Analysis: Charge Density. Phenyl Rings. Both the carbon−carbon and carbon−hydrogen bonds in the phenyl rings display relatively high values of ρ and negative values of $\nabla^2\rho$ at the corresponding BCPs (Table 6). Indeed, prominent local charge concentration (solid lines in Figure 3a) clearly indicates the covalent nature of these interatomic interactions. The bond ellipticities, $\epsilon = [\lambda_1/\lambda_2 - 1]$, for the carbon−carbon bonds (ϵ at ∼0.2) reflect the existence of the π-bonding interactions in the plane normal to the phenyl ring and are in good agreement with the theoretical estimation $\epsilon = 0.23$ for benzene.[4a]

Carbonyl Ligands. The charge densities, ρ, at the carbonyl BCPs are the highest among all BCPs in the molecule (Table 6), which is indicative of shared (covalent) interatomic interactions. However, the Laplacian of ρ at these points is positive, indicating a *local* charge depletion, as if a closed-shell interaction takes place. This apparent dichotomy is observed (with one exception[49]) in a number of theoretical studies of the CO molecule,[4a,50] for which a quantitative comparison can be made, and is evident from theoretical studies both of CO adducts with

(47) (a) Cioslowski, J.; Mixon, S. T.; Edwards, W. D. *J. Am. Chem. Soc.* **1991**, *113*, 1083. (b) Cioslowski, J.; Mixon, S. T. *J. Am. Chem. Soc.* **1992**, *114*, 4382. (c) Cioslowski, J.; Mixon, S. T. *Can. J. Chem.* **1992**, *70*, 443. (d) Cioslowski, J.; Edgington, L.; Stefanov, B. B. *J. Am. Chem. Soc.* **1995**, *117*, 10381. (e) Abramov, Yu. A. *J. Phys. Chem.* **1997**, *A101*, 5725.

(48) Howard, S. T.; Mallinson, P. R. *LSPROP: A One-Electron Properties Package for LSMOL;* 1992 (unpublished).

(49) Bo et al.[9d] have used SCF and CASSCF methods in calculations of topology for molecular CO. The former show a value of ρ at the BCP much lower than other calculations using HF[4a,50] and density functional methods,[50] and our experimental values for the carbonyl ligand. The CASSCF calculations show values of both ρ (much higher) and $\nabla^2\rho$ (opposite sign!) in marked disagreement with other determinations.

(50) (a) Aray, Y.; Rodriguez, J. *Can. J. Chem.* **1996**, *74*, 1014. (b) Aray, Y.; Rodriguez, J.; Lopez-Boada, R. *J. Phys. Chem.* **1997**, *101*, 2178.

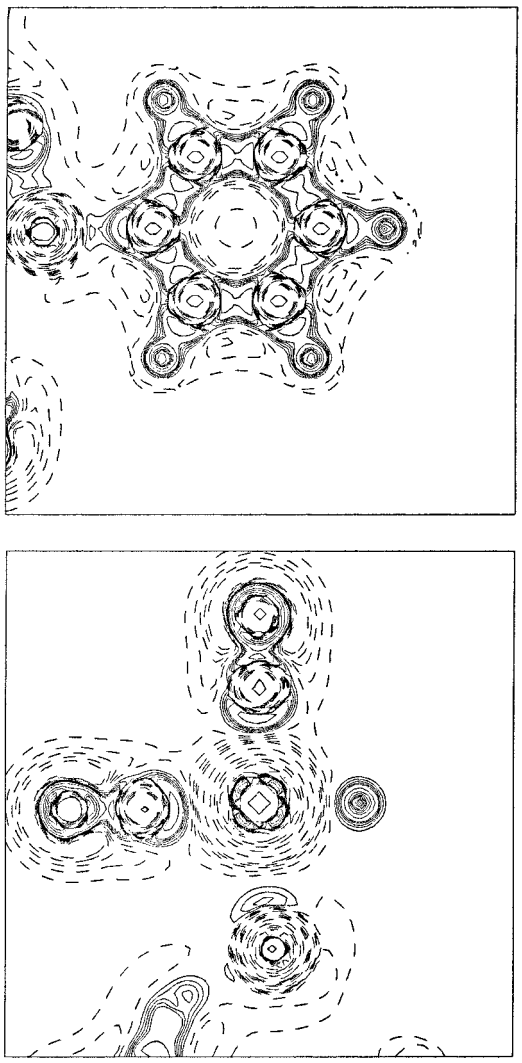

Figure 3. Static $-\nabla^2\rho$ maps in the planes defined by atoms: (a) C(5), C(8), C(10); (b) Mn, H(1), C(2). Contour values are ±2, ±4, ±6, ±8, and ±10 e/Å^5 increasing in powers of 10 to ±1000 e/Å^5. Positive and negative contours are represented by solid and dashed lines, respectively.

main group Lewis acids[51] and of transition metal carbonyl complexes,[9a,c] for which only a qualitative comparison is available by inspection of $\nabla^2\rho$ maps.

The C≡O bond falls into Bader's intermediate bond category,[4a] wherein its BCP lies close to the $\nabla^2\rho$ nodal plane. Thus, the present topological study of this bond type provides a good test of the quality of the experimental data. The properties of ρ at the BCPs in all the carbonyls of the $HMn(CO)_4PPh_3$ molecule are in approximate quantitative agreement with the theoretical observations[4a,50a] on carbon monoxide.[52] Thus, the BCPs in all carbonyls are located within the inner shell of local charge depletion at a carbon atom, adjacent to the nodal surface in the $\nabla^2\rho$ distribution, accounting for the positive Laplacian at the BCP. At the same time, again consistent with theoretical observations,[4a,50] a large area of local charge concentration (solid lines, Figure 3b) in the internuclear region between carbon and oxygen, lies within the oxygen atom basins in each carbonyl group, which is consistent the shared interatomic interaction suggested by the high charge density at the BCP. This clearly points to the fact that it is important to examine the properties of the charge density in the *whole internuclear region* and not solely focus on the BCP in order to obtain a complete picture of the chemical bond.

At first consideration the changes in ρ at the BCP on going from molecular CO to carbonyl groups in $HMn(CO)_4PPh_3$ may seem quite small, but realistically only small quantitative changes should be expected. Changes in C−O distance are of the order of 0.03 Å, and even the characteristic change in IR stretching frequency is only from 2143 to 2061−1957 cm^{-1}. A clearer picture of the charges in the charge density distribution can be obtained by also comparing (theoretical values for) formally double bonded species $H_2C{=}O$ and $O{=}C{=}O$.[4a] It is clear that there is only a small decrease in ρ at the BCP despite the formal decrease in bond order [ρ: CO, 3.42; H_2CO, 2.91; CO_2, 3.26; $HMn(CO)_4PPh_3$, 3.19(2)−3.24(3) e Å^{-3}] and that the values for the carbonyls in $HMn(CO)_4PPh_3$ are quite consistent with weakening of the CO bond upon coordination. However, no significant differences between the coordinated carbonyls are observed (Table 6). The value of $\nabla^2\rho$ is much more sensitive to the bond order [$\nabla^2\rho$: CO, 23.6; H_2CO, 11.1; CO_2, 3.6; $HMn(CO)_4PPh_3$, 6.7(10)−16.4(9) e Å^{-5}], since, though occupied bonding π MOs do not contribute charge density at the BCP, they do decrease the magnitudes of negative curvatures λ_1 and λ_2 (and increase the kinetic energy density G[53]) at this point. From this point of view, the values of $\nabla^2\rho$ at the BCPs obtained for the carbonyl groups in $HMn(CO)_4PPh_3$ reflect the formal bond order being between two and three.

Metal−Ligand Bonding. The manganese−ligand bonds display a *local* depletion of electrons (positive Laplacian) and low but *quite significant* values of the charge density at the BCPs (Table 6). These properties most closely approximate the definition of a closed-shell interaction (vide supra). The interactions differ from Bader's intermediate bond definition in that the positions of the BCPs are relatively far from nodal surfaces in $\nabla^2\rho$ distribution. However, one cannot ignore the appreciable charge accumulation associated with these bonds. For example, the values of ρ for the Mn−C bond BCPs approach those of the (covalent) phosphine P−C bonds.

The Mn−L bonds, particularly Mn−C, in the present study show values of ρ and $\nabla^2\rho$ at the BCP very similar to those calculated theoretically[51] for the simple σ-donor/acceptor B−C bond in $OC{\rightarrow}BH_3$ and differ primarily in the almost coincidence of interatomic surfaces with nodal surfaces in $\nabla^2\rho$ that occurs only for the latter. Thus, as for the C≡O bonds discussed previously, a complete bonding picture for the Mn−L bonds is attained by considering the properties of the *whole internuclear region* and not just the BCP. The Laplacian distribution is positive (dashed lines in Figure 3b) over an almost spherical region between Mn and the ligands, illustrating the local charge depletion from this region with concomitant charge transfer to regions of negative $\nabla^2\rho$. In the outer valence shell of charge concentration (VSCC) of the Mn atom, the regions of preferable local electron concentration are associated with the d orbitals of (octahedral) t_{2g} symmetry, where $\nabla^2\rho$ displays negative lobes directed toward the faces of the octahedron defined by the six ligands. (Figure 3b displays traces of these lobes as solid lines in the C(2)−Mn−H(1) plane.) This observation is qualitatively

(51) Jonas, V.; Frenking, G.; Reetz, M. T. *J. Am. Chem. Soc.* **1994**, *116*, 8741.

(52) Exact quantitative agreement should not be expected, not least because of the *chemical* differences between molecular CO and a carbonyl ligand (vide infra).

(53) (a) Full details of the experimental kinetic energy density analysis of the C≡O bonds is provided in Supporting Information. The analysis was conducted according to the approach of Abramov.[53b] (b) Abramov, Yu. A. *Acta Crystallogr.* **1997**, *A53*, 264.

consistent with the crystal field effect in the Mn complex and is consistent with the deformation density distribution (vide supra).

The ellipticity $\epsilon \sim 0.1$ determined for the BCPs associated with the Mn−C1 and Mn−C3 bonds suggest that the π-back-donation is slightly different in the two orthogonal planes of the CO π^* orbitals. This is perhaps as a result of the noticeable deviation of these Mn−C bonds away from a mutually trans orientation and toward the hydride. It is also of interest to note that the charge density at the BCP is greater for the two bonds, Mn−C(2) and Mn−C(4), that are trans to the phosphine and hydride, respectively, than for the mutually pseudo-trans pair Mn−C(1) and Mn−C(3).

For the Mn−H bond the only available comparisons are with theoretical studies of transition metal polyhydrides.[9i,10b,c,e,g] Of these a quantitative comparison of the BCP, etc. is only possible for VH_5,[9i] for which the accumulation of charge density at the BCP compares well [ρ, 0.651(21) vs 0.682−0.877 e/Å^3 for VH_5], whereas $\nabla^2\rho$ values at the BCP are higher than for VH_5 [$\nabla^2\rho$ 5.30(9) vs −0.31 to 1.04 e/Å^5 for VH_5]. In these two studies the M−H bond lengths (1.58−1.72 Å) and positions of BCP (ca. 1.02−1.07 Å from H) are similar. Thus, $\nabla^2\rho$ values suggest that the BCPs for VH_5 lie closer to the nodal plane in $\nabla^2\rho$ than for $HMn(CO)_4PPh_3$. Gillespie et al. conclude[9i] that the V−H bonds in VH_5 are predominantly covalent in character. However, in accord with the predominantly positive distribution of $\nabla^2\rho$ in the region between Mn and H (Figure 3b), including at the BCP, a description of Mn−H bonding as primarily closed shell in nature but with some covalent character, i.e., a dative bond, seems most appropriate. A qualitative comparison is also possible with the work of Hall and co-workers in which the Laplacian of ρ has been used in the interpretation of bonding in a number of metal polyhydride systems. From those studies, the $-\nabla^2\rho$ maps for $IrH_5(PMe_3)_2$[10c] appear very similar to ours for $HMn(CO)_4PPh_3$, i.e. suggesting dative M−H bonds. In contrast, the M−H bonds in $[ReH_4(PH_3)_4]^+$ [10e] and $CpReH_6$[10g] show a local electron concentration linking the Re and H atoms indicative of a pronounced covalent character. Thus, it appears that the extent of the covalent contribution to M−H bonding can vary from dative (i.e., donor−acceptor) with only a small covalent contribution, as in *cis*-$HMn(CO)_4PPh_3$, to predominantly covalent.

Quantitative comparisons with other studies for the metal−phosphine bond are not available, though the Laplacian distribution in the region of the Mn−P bond in the present study is in qualitative agreement with the $-\nabla^2\rho$ maps presented by Hall and co-workers for $[ReH_4(PH_3)_4]^+$ [10e] and $ReH_2(SiH_3)CO(PH_3)_2$.[10b]

C−H···H−M Hydrogen Bond. There is a bond path[4a] connecting hydride H(1) with the ortho hydrogen H(22) of one phenyl ring. The corresponding (3, −1) CP has associated with it a low value of ρ and positive $\nabla^2\rho$ (Table 6), which according to the theory of atoms in molecules[4] suggests the presence of a closed-shell interaction consistent with an intermediate or long hydrogen bond. In light of our earlier comments, the bond path and CP are a necessary but perhaps not sufficient condition for an attractive bonding interaction between the two hydrogens. However, the values of ρ and $\nabla^2\rho$ at the CP lie within the ranges suggested to be indicative of hydrogen bonding[54] and applied by Popelier to N−H···H−B hydrogen bonds.[54b]

Furthermore, when taken in conjunction with the geometric and electrostatic evidence (vide supra) this observation provides very strong support for the existence of an intramolecular hydrogen bond C−H(22)···H(1)−Mn between the electrophilic, H(22), and nucleophilic, H(1), hydrogens.

Summary of Topological Analysis of Charge Density. Overall, one can conclude that while the C−C, C−H, and P−C bonds are obviously shared covalent interactions, the C≡O bonds and M−L bonds lie between the extremes of strictly shared and closed-shell interactions. The C≡O bonds (formally defined[4a] as intermediate bonds) lie closer to the shared covalent interaction description, as demonstrated most markedly by the very large value of ρ at the BCP, indicating an accumulation of charge consistent with a covalent bond. The M−L bonds lie closer to the closed-shell extreme of bonding descriptions and deviate from this description (toward a shared interaction) only in the accumulation of charge noted in the ρ values at the BCP. The M−L bonds can best be described as dative bonds. Finally, the topology of the charge density supports geometric and electrostatic considerations in allowing characterization of an uncommon C−H···H−M hydrogen bond.

Topological Analysis: Laplacian of the Charge Density. Further understanding of the chemical information presented in the charge density can be provided by a study of the topology of the $-\nabla^2\rho$ distribution.[4a] This allows location of bonded and nonbonded (lone pair) *local* concentrations of electrons, which although not displayed in the topology of a total charge density, ρ, are consistent with the features found in the deformation density. The CPs of the Laplacian can be used in analysis of the interactions of the atoms in the crystal in a generalized Lewis acid−base manner, i.e., in terms of their electrophilicity or nucleophilicity. An extensive search for such critical points in the VSCC of the Mn atom together with a limited analysis of such CPs associated with the ligand atoms has been conducted. To our knowledge this is the first such study based upon an *experimental* charge density distribution. Further details of this aspect of the study are presented in the Supporting Information (Tables S4, and S5) and will be described only briefly here with an emphasis on the acid−base nature of the metal−ligand interactions.

The complete atomic graph[4a] for the Mn atom illustrating all CPs in the VSCC has been elucidated[55] (Figure 4). The pattern of electron concentration (t_{2g} orbitals) and depletion (e_g orbitals) within the Mn VSCC is qualitatively consistent with expectations from crystal field theory and in agreement with the deformation density (vide supra). The location and properties of both the bonded and nonbonded concentrations of charge for the CO ligand shows very good agreement with theoretical studies of the CO molecule.[49]

The subset of CPs in $-\nabla^2\rho$ that has been located allows the following picture of the Lewis acid−base nature of the $HMn(CO)_4PPh_3$ molecule to be developed. Metal−ligand bonding takes place, first of all, through the alignment of the regions of the local charge concentration (base) with those of local charge depletion (acid) (Figure 4). In the principal (σ) interactions, the former regions are the nonbonded charge concentrations (lone pairs) of the carbon atoms in the carbonyls and of the phosphorus and the hydride charge density (all (3, −3) CPs in

(54) (a) Koch, U.; Popelier, P. L. A. *J. Phys. Chem.* **1995**, *99*, 9747. (b) Popelier, P. L. A. *J. Phys. Chem. A* **1998**, *102*, 1873.

(55) (a) The search for CPs in $-\nabla^2\rho$ in the Mn atom VSCC is complicated for several reasons. First, the Laplacian of the charge density of a transition metal has much more complicated net of CPs, than its charge density, and fully recovering this net requires the application of a more reliable algorithm[50b,55b,c] than the conventional Newton−Raphson method used in the present study. Second, the total charge density in the region of the VSCC of the Mn atom is very high causing a large contribution to the errors in $\nabla^2\rho$ in this region. (b) Popelier, P. L. A. *Chem. Phys. Lett.* **1994**, *228*, 160. (c) Cioslowski, J.; Nanayakkara, A. *Chem. Phys. Lett.* **1994**, *219*, 151.

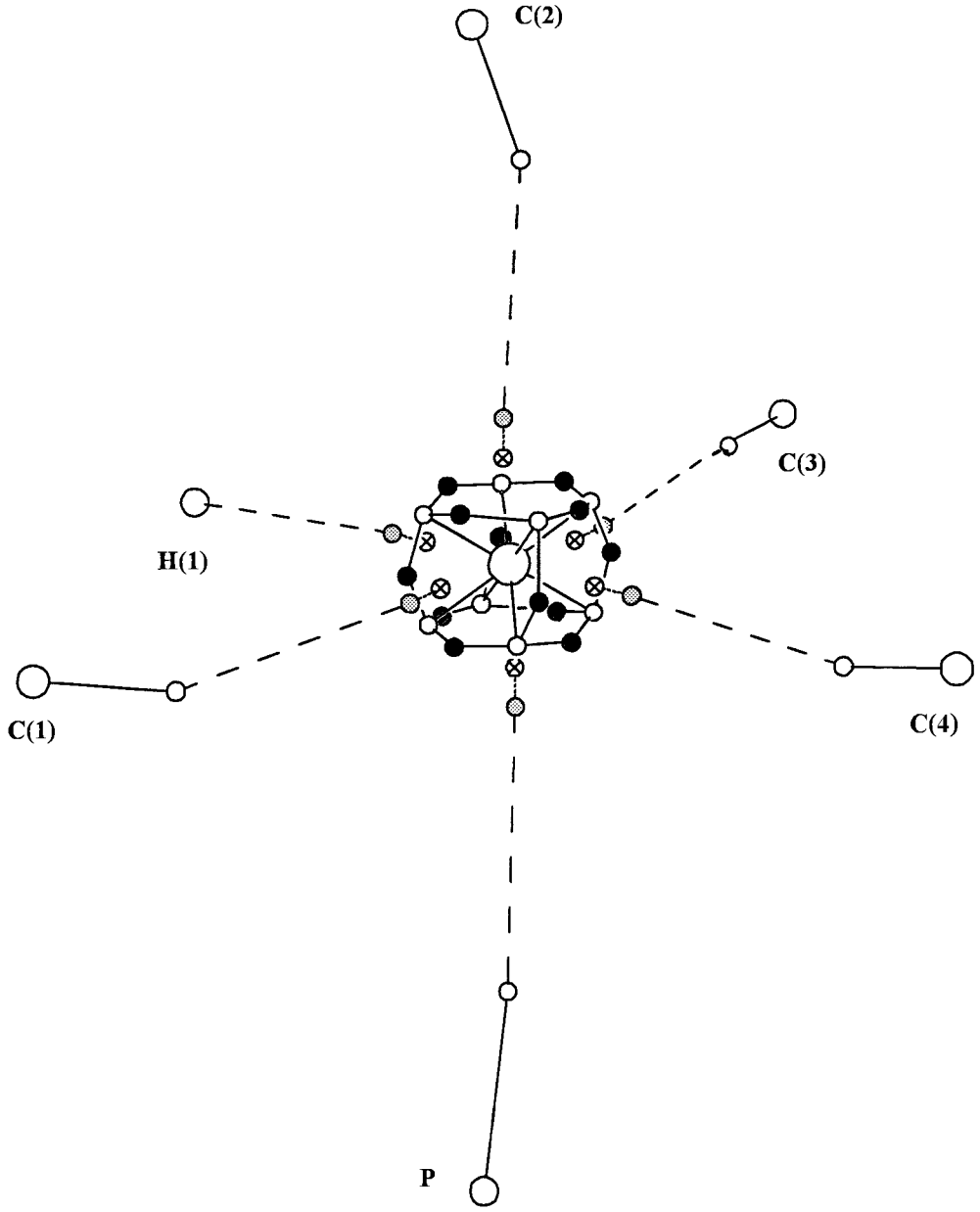

Figure 4. Selected critical points in $-\nabla^2\rho$ and atomic graph of the Mn atom (see text). Open, black, crossed, and gray circles mark the (3, −3), (3, −1), (3, +1), and (3, +3) critical points in $-\nabla^2\rho$, respectively. Large open circles correspond to density accumulation at the nuclear positions, and small open circles denote the position of atomic lone pairs.

$-\nabla^2\rho$). The latter regions are the (3, +1) and (3, +3) CPs in $-\nabla^2\rho$ at the location of the e_g d-orbitals of the Mn atom. In the secondary (π) interactions, the nonbonded electron concentration over the t_{2g} orbitals of the Mn atom, acting as a base, is directed to the regions of the carbonyl π^* MO localization, which act as a weak acid. However, the presence of this π-acid−base interaction (or a π-back-donation from Mn to CO π^* MOs in the previous terminology) is manifested in the covering of the whole area of the torus of charge depletion, which encircles the carbon nucleus in free CO, by a surface of a low charge concentration in the carbonyls in the $HMn(CO)_4PPh_3$ crystal, similar to that observed in theoretical studies of $Fe(CO)_5$[9a,c] and $Mn_2(CO)_{10}$.[9j]

Conclusions

This study reports the experimentally determined charge density of *cis*-$HMn(CO)_4PPh_3$, the first such a study of a transition metal hydride compound, using X-ray data from a CCD area detector. It is one of very few topological studies to date of the experimental charge density for a transition metal complex, and the first involving a topological study of the Laplacian.

The coordination geometry of *cis*-$HMn(CO)_4PPh_3$ deviates from octahedral in that the trans pair of carbonyls are displaced toward the hydride ligand which is cis to them. There is a short contact between the hydride and an ortho hydrogen of one phenyl ring [2.101(3)]. The geometry of the C−H···H−Mn interaction suggests the presence of a relatively weak hydrogen bond between electrophilic and nucleophilic hydrogens (see effective atomic charges, Table 4), which give rise to an electrostatic interaction energy of 5.7 kcal/mol in the crystal. The classification of this interaction as a hydrogen bond is further supported by the bond path that lies between the two hydrogens and the properties of the charge density at the bond critical point.

Examination of the deformation density clearly illustrates the σ-donor nature of the phosphine and hydride ligands. The hydride ligand is hydridic in nature and carries a small negative charge (ca. −0.4e, cf. phenyl hydrogens ca. +0.3e). The σ-donor/π-acceptor nature of the carbonyls is evident not only from the deformation density, but from the greater negative (monopole) charges associated with the carbons than the oxygens, consistent with the predominant localization of the π* acceptor orbitals on carbon. It is also noted that the while derived d-orbital populations of Mn are qualitatively consistent with a crystal field theory description of metal−ligand bonding, the substantially nonzero populations of the d_{z^2} and $d_{x^2-y^2}$ orbitals suggests some (dative) covalent contribution to the Mn-L bonds. Furthermore, the occupancies of the d_{yz}- and d_{xy}-orbitals involved in π-back-donation to three carbonyl ligands, are significantly less than that of the d_{xz}-orbital, which interacts with only two carbonyls.

In addition to confirming the σ-donor/π-acceptor nature of the carbonyls and the σ-donor−acceptor nature of the H−Mn and PPh_3P−Mn bonds, analysis of the topology of the charge density, ρ, and its Laplacian, $\nabla^2\rho$, has allowed a visualization of the specific acid−base interactions that comprise the metal−ligand bonds. Furthermore, on the scale of bond types which range from shared covalent at one extreme to closed-shell (e.g., ionic and hydrogen bonds) at the other, it is clear that the metal ligand bonds in *cis*-$HMn(CO)_4PPh_3$ lie closer to the closed-shell extreme, but include a significant component of covalency, i.e., a dative bonding description. The C≡O bonds of the carbonyls, on the other hand, lie closer to the shared covalent extreme, but are somewhat displaced toward the closed-shell description.

The present study shows the potential of combining recent advances in instrumentation and software for the experimental analysis of chemical bonding via the charge density distribution in ever more challenging systems. Current work in progress includes studies of agostic and hydrogen-bonded transition metal compounds.

Acknowledgment. L.B. acknowledges support for this work from the donors of the Petroleum Research Fund, administered by the American Chemical Society. Purchase of the Siemens SMART diffractometer was funded in part by NSF Grant No. CHE-9309690. Research at Brookhaven National Laboratory was carried out under Contract DE-AC02-76CH00016 with the U.S. Department of Energy and supported by its Division of Chemical Sciences, Office of Basic Energy Sciences. We thank C. Koehler III for technical assistance with the neutron diffraction study.

Supporting Information Available: Tables of neutron and X-ray atomic coordinates and displacement parameters, multipole parameters, properties of the charge density at the critical points in $-\nabla^2\rho$, experimental kinetic energy densities at the carbonyl BCPs and residual density maps (21 pages). Ordering information is given on any current masthead page.

IC9809660